Journal of Physics G: Nuclear and Particle Physics

Many-body cascade calculation of final state interactions in ${}^{12}_{\Lambda}$C nonmesonic weak decay

To cite this article: I Gonzalez *et al* 2011 *J. Phys. G: Nucl. Part. Phys.* **38** 115105

View the article online for updates and enhancements.

You may also like

- Nonmesonic Hyperon Weak Decay Spectra in ^{12}C
I Gonzalez, A Deppman, S Duarte et al.
- Experimental review of hypernuclear physics: recent achievements and future perspectives
A Feliciello and T Nagae
- Magnetism in Isolated and Binary White Dwarfs
D. T. Wickramasinghe and Lilia Ferrario

This content was downloaded from IP address 143.107.135.170 on 29/08/2023 at 22:52

J. Phys. G: Nucl. Part. Phys. **38** (2011) 115105 (16pp) doi:10.1088/0954-3899/38/11/115105

Many-body cascade calculation of final state interactions in $^{12}_{\Lambda}$C nonmesonic weak decay

I Gonzalez[1,2], C Barbero[3,4], A Deppman[1], S B Duarte[5], F Krmpotić[4,6] and O Rodriguez[1,2]

[1] Instituto de Física, Universidad de São Paulo, São Paulo, Brazil
[2] Instituto de Tecnologías y Ciencias Aplicadas, Havana, Cuba
[3] Departamento de Física, Facultad de Ciencias Exactas, Universidad Nacional de La Plata, C.C. 67, 1900 La Plata, Argentina
[4] Instituto de Física La Plata, CONICET, 1900 La Plata, Argentina
[5] Centro Brasileiro de Pesquisas Físicas, Rua Dr Xavier Sigaud 150, CEP 22290-180, Rio de Janeiro-RJ, Brazil
[6] Facultad de Ciencias Astronómicas y Geofísicas, Universidad Nacional de La Plata, 1900 La Plata, Argentina

E-mail: barbero@fisica.unlp.edu.ar

Received 29 December 2010
Published 23 September 2011
Online at stacks.iop.org/JPhysG/38/115105

Abstract

We study the nonmesonic weak decay (NMWD) $\Lambda N \rightarrow nN$ of $^{12}_{\Lambda}C$ hypernucleus induced by one nucleon $N = n, p$. The whole process is described by two coupled models: one for the primary NMWD of Λ hyperon in the nuclear environment, and the other taking into account the final state interactions (FSI) of the two outgoing nucleons within the residual nucleus. The NMWD dynamics is represented by the one-meson-exchange potential with usual parametrization, while the independent-particle shell model is used as the nuclear structure framework. The FSI are accounted for by a time-dependent multicollisional Monte Carlo cascade scheme, implemented within the CRISP code (Collaboration Rio-São Paulo), which describes in a phenomenological way both the nucleon–nucleon scattering inside the nucleus and the escaping of nucleons from the nuclear surface. An evaporation phase is included to cool down the cascade residual nucleus as well. We analyze the single-nucleon kinetic energy spectra, and the two-nucleon coincidence spectra as a function of both: (i) the sum of the kinetic energies and (ii) the opening angle. The theoretical results are compared with recent data from KEK and FINUDA experiments, obtaining fairly good agreement for inclusive and exclusive kinetic energy spectra. Further theoretical improvements are required to explain angular distributions.

(Some figures in this article are in colour only in the electronic version)

 © 2011 IOP Publishing Ltd Printed in the UK & the USA

1. Introduction

In recent years, there has been a renewed interest in the issue of strangeness in nuclear structure and hypernuclear decay. This interest stems from the observation of bound states in several hypernuclei, such as ${}^{10}_{\Lambda}$B, ${}^{12}_{\Lambda}$C, ${}^{28}_{\Lambda}$Si, ${}^{89}_{\Lambda}$Y, ${}^{139}_{\Lambda}$La, ${}^{208}_{\Lambda}$Pb, ${}^{209}_{\Lambda}$Bi, and ${}^{238}_{\Lambda}$U [1–7], which are topics of investigation in present-day experiments. From the theoretical side, many models have been developed in recent years to seek some enlightenment on the Λ-shell structure. Indeed, static calculations based on studies of the hyperon–nucleon potential [8, 9], chiral perturbation theory [10] and statistical models [11] have provided some insights on the properties of hypernuclei such as their mass shifts, wavefunctions, fissioning path and attachment probabilities of hyperons in nuclei. In the last ten years, interest on kaon-induced reactions has grown since the observation of new nuclear Λ-bound states, experimentally detected through the excitation of the target nucleus by an incident polarized kaon beam. As a matter of fact, new phenomena related to the inclusion of a Λ in the nuclear structure, such as halo effects [12], have been discussed. The presence of hyperons inside the nucleus can lead to weakly bound states, making possible the observation of halo nuclei beyond the neutron drip line. A typical example is ${}^{6}_{\Lambda}$He. Although ${}^{5}_{\Lambda}$He is unbound by 0.89 MeV above the threshold for the ${}^{5}_{\Lambda}\mathrm{He} \rightarrow \alpha + n$ reaction, the ${}^{6}_{\Lambda}$He ground state is bound by 0.17 MeV against the breaking into ${}^{5}_{\Lambda}\mathrm{He} + n$ [12].

Besides having these interesting features, the hypernuclear systems offer us the opportunity to study the nonmesonic weak decay (NMWD) $\Lambda N \rightarrow nN$, where $N = p, n$. This is the dominant hypernuclear decay mode, since the mesonic channel $\Lambda \rightarrow \pi N$ is Pauli blocked inside the nuclear medium. It can be induced either by a neutron ($\Lambda n \rightarrow nn$) or by a proton ($\Lambda p \rightarrow np$) with decay widths Γ_n and Γ_p, respectively. In the course of the last two decades, remarkable efforts have been invested in trying to solve the so-called NMWD puzzle. This puzzle is related to the large discrepancy between earlier experimental data and theoretical predictions for proton and neutron kinetic energy spectra. Recent advances on the NMWD have led to the solution of this longstanding discrepancy. From the experimental side, more precise measurements have been performed of single-nucleon spectra [13, 14], as well as the two-nucleon coincidence spectra, as a function of both: (i) the sum of the kinetic energies and (ii) the opening angle have been analyzed experimentally for the first time [15, 16]. Simultaneously, it was shown through the theoretical calculations that the final state interactions (FSI) play a very important role in the NMWD, to the extent that they are crucial to make the calculated Γ_n/Γ_p decay ratios compatible with experimental determinations [17–21].

There are several recipes at our disposal in the literature to describe the FSI between the primary nucleons nN and the residual nucleus. Basically, they are phenomenological models, dealing with either an intranuclear cascade code (INC) [17–20], or with an optical potential [22–24]. In the first case the nucleon propagation inside the residual nucleus is simulated by a time-independent Monte Carlo code. The whole cascade process is reproduced by the superposition of a semi-classical path of nucleons produced in the weak decay (together with others generated by secondary collision chains) until they leave the nucleus. In the second case, the optical potentials play the role of the nuclear medium to the nucleons emerging from the weak decay. Moreover, recently the FSI were described microscopically in the context of the nuclear matter formalism with the help of the local density approximation and the ground state correlations. The latter were evaluated within the first-order perturbation theory where the residual interaction has been treated at the same footing as the weak decay mechanism [21, 25].

The many-body cascade calculation proposed in [26, 27] for the rapid phase of the nuclear reaction is a time-dependent multicollisional Monte Carlo cascade scheme, implemented in

the CRISP code (Rio-São Paulo Collaboration), and which includes an evaporation phase as well. It takes into account the dynamical evolution of the multicollisional nucleon–nucleon processes, and has been used successfully for many other purposes [28–31]. The dynamical characteristics of the calculation allow one to consider the rapid and pre-equilibrium phases within a single theoretical approach, in contrast with standard calculations [32–34].

The main aim of this work is to analyze to which extent the FSI, accounted for by means of the CRISP code, modify the spectra obtained within the independent particle shell model (IPSM) [35–40], and to find out to what extent it is possible to explain the experimental data. The IPSM spectra are used to start up the cascade process. Unlike the INC calculation from [17–20] our time-dependent multicollisional approach describes the propagation of nucleons inside the residual nucleus following the whole time evolution of the many-body system after the primary nucleon excitation induced by the NMWD event. Another important characteristic of our cascade calculation lies on the possibility of determining the final thermal equilibrated residual-nucleus configuration at the end of the rapid phase which is the starting point for the subsequent evaporation phase of the hypernucleus decaying process.

There have been recent reports at KEK [13], and at FINUDA [14] on the measurements of two-body induced NMWD $\Lambda NN \to nNN$ with a branching ratio as large as $\cong 30\%$. These measurements are consistent with the theoretical estimations made by Bauer and Garbarino [25], which are based on previously developed formalism for the $2N$ decay within the framework of the Fermi gas model [41]. We do not know how this process is described within the IPSM. In fact, nobody has done this so far, and we are working in this direction. Such information is required, in turn, to start the corresponding Monte Carlo cascade sequence to take into account the FSI. It is for this reason that we do not discuss the $\Lambda NN \to nNN$ decay here.

The paper is organized as follows. In section 2 the formulation for the NMWD spectra is presented, representing the decay mechanism by the one-meson-exchange potential (OMEP) and employing the IPSM as the nuclear structure framework. The corresponding numerical results are presented as well. Some of these results are used in section 3 to start up the internuclear cascade phase which is implemented by the CRISP code in order to incorporate the FSI effect to the outgoing nucleon state. In this way, we obtain our final results for the NMWD spectra. Section 4 is devoted to our conclusions and final remarks.

2. The primary NMWD model

Here, we sketch the main ingredients of the model that is used as the first-order approximation to describe the NMWD spectra, and the transition rates in ${}^{12}_{\Lambda}\mathrm{C}$. At the same time this model plays an essential role in triggering the cascade phase, as it provide us with information on the initial nucleons, specifying the probability for their relative momentum and the corresponding opening angle.

Within the IPSM the following assumptions are made [35–40]:

(1) The initial hypernuclear state is taken as a hyperon Λ in a single-particle state $j_\Lambda = 0s_{1/2}$ weakly coupled to an $(A-1)$ nuclear core of spin J_C, i.e. $|J_I\rangle \equiv |(J_C\, j_\Lambda) J_I\rangle$.
(2) When the nucleon $(N = p, n)$ inducing the decay is in the single-particle state $j_N (j \equiv nlj)$, the final residual nucleus states are $|\alpha_N J_F\rangle \equiv |(J_C\, j_N^{-1}) J_F\rangle$.
(3) We adopt the simplest version of the IPSM, in which all relevant particle states are assumed to be stationary, and the liberated energy is

$$\Delta_N^j = \Delta + \varepsilon_\Lambda + \varepsilon_N^j, \tag{1}$$

where ε's are single-particle energies, and $\Delta = \mathrm{M}_\Lambda - \mathrm{M}$. (The non-stationary version of the IPSM is discussed in [37].)

Under above conditions the primary NMWD decay rate can be cast in the form

$$\Gamma_N = \sum_j \Gamma_N^j; \quad \Gamma_N^j = \sum_{J=|j-1/2|}^{J=j+1/2} F_{NJ}^j \mathcal{R}_{NJ}^j. \tag{2}$$

The nuclear structure information is contained in the spectroscopic factor

$$\begin{aligned} F_{NJ}^j &= \hat{J_I}^{-2} \sum_{J_F} |\langle J_I || \left(a_{j_N}^\dagger a_{j_\Lambda}^\dagger\right)_J || J_F\rangle|^2 \\ &= \hat{J}^2 \sum_{J_F} \begin{Bmatrix} J_C & J_I & j_\Lambda \\ J & j_N & J_F \end{Bmatrix}^2 \left|\left\langle J_C \middle|\middle| a_{j_N}^\dagger \middle|\middle| J_F \right\rangle\right|^2, \end{aligned} \tag{3}$$

with the notation $\hat{J} = \sqrt{2J+1}$.

The quantity $\mathcal{R}_{NJ}^j$ encloses both the dynamics and the kinematics of the NMWD, and can be expressed generically as

$$\mathcal{R}_{NJ}^j = \sum_L \int \mathcal{T}_{NJL}^j(p) \mathcal{O}_L^2(P) \mathrm{d}\Omega, \tag{4}$$

where

$$P = \sqrt{(A-2)\left(2\mathrm{M}\Delta_N^j - p_n^2 - p_N^2\right)}, \tag{5}$$

and

$$p = \sqrt{\mathrm{M}\Delta_N^j - \frac{A}{4(A-2)} P^2}, \tag{6}$$

are, respectively, relative and c.m. momenta, with p_n, and p_N, being the momenta of the emitted particles.

The dynamics is contained in

$$\mathcal{T}_{NJL}^j(p) = \sum_{Sl\lambda T} |\mathcal{M}(plPL\lambda SJ\mathsf{T}; j_\Lambda j_N J \mathrm{t}_{\Lambda N})|^2, \tag{7}$$

where $\boldsymbol{\lambda} = \boldsymbol{l} + \boldsymbol{L}$, with $\boldsymbol{l}$ and $\boldsymbol{L}$ being, respectively, relative and c.m. angular momenta, $\mathsf{T} \equiv \{TM_T, M_T = m_{t_\Lambda} + m_{t_N}\}$, and $\mathrm{t}_{\Lambda N} \equiv \{t_\Lambda = 1/2, m_{t_\Lambda} = -1/2, t_N = 1/2, m_{t_N}\}$, with $m_{t_p} = 1/2$, and $m_{t_n} = -1/2$, where we have assumed that the $\Lambda N \to nN$ interaction occurs with the isospin change $\Delta T = 1/2$. Moreover,

$$\mathcal{M}(plPL\lambda SJ\mathcal{T}; j_\Lambda j_N J \mathrm{t}_{\Lambda N}) = \tfrac{1}{\sqrt{2}}\left[1 - (-)^{l+S+T}\right](lL\lambda SJ\mathcal{T}|V(p)|j_\Lambda j_N J \mathrm{t}_{\Lambda N}), \tag{8}$$

where (here and henceforth) the ket $|)$, unlike $|\rangle$, indicates that the state is not antisymmetrized, and $V(p)$ is the transition potential.

The kinematic is enclosed in (1) the overlap between the c.m. radial wavefunctions R_{0L} of the bound particles and j_L of the outgoing particles

$$\mathcal{O}_L(P) = \int R^2 \, \mathrm{d}R j_L(PR) \mathrm{R}_{0L}(b/\sqrt{2}, R), \tag{9}$$

where b is the harmonic oscillator size parameter; and (2) the phase space factor $\mathrm{d}\Omega$, which depends on the spectra that one is interested in.

In this work, we need the NMWD spectra as a function of (1) the momentum p_N and the kinetic energy E_N of the final nucleon state, (2) the kinetic energy sum $E_{nN} = E_n + E_N$

of the emitted particles and (3) the corresponding opening angle θ_{nN}. They are obtained by performing derivatives on these variables in the appropriate equation for Γ_N that are presented below, where we will use the compact notation

$$\mathcal{I}_N^j(p, P) = \sum_{J=|j-1/2|}^{J=j+1/2} F_{NJ}^j \sum_L \mathcal{T}_{NJL}^j(p)\mathcal{O}_L^2(P). \tag{10}$$

- Kinetic energy sum $E_{nN} = E_n + E_N$ spectrum

$$\Gamma_N^j = \frac{4\mathrm{M}^3}{\pi}\sqrt{A(A-2)^3}\int_0^{\tilde{\Delta}_N^j} \mathrm{d}E_{nN}\sqrt{\left(\Delta_N^j - E_{nN}\right)\left(E_{nN} - \tilde{\Delta}_N^j\right)}\mathcal{I}_N^j(p, P), \tag{11}$$

with

$$\tilde{\Delta}_N^j = \Delta_N^j \frac{A-2}{A}. \tag{12}$$

- Kinetic energy E_N and opening angle θ_{nN} spectra

$$\Gamma_N^j = (A-2)\frac{8\mathrm{M}^3}{\pi}\int_{-1}^{+1} \mathrm{d}\cos\theta_{nN}\int_0^{\tilde{E}_N^j} \mathrm{d}E_N\sqrt{\frac{E_N}{E'_N}}E_n\mathcal{I}_N^j(p, P), \tag{13}$$

where

$$E'_N = (A-2)(A-1)\Delta_N^j - E_N[(A-1)^2 - \cos^2\theta_{nN}], \tag{14}$$

$$E_n = \left[\sqrt{E'_N} - \sqrt{E_N}\cos\theta_{nN}\right]^2(A-1)^{-2}, \tag{15}$$

and

$$\tilde{E}_N^j = \frac{A-1}{A}\Delta_N^j. \tag{16}$$

Throughout the integration one has to enforce the condition

$$E'_N > E_N\cos^2\theta_{nN}. \tag{17}$$

It might be worth noting that, while E'_N does not have a direct physical meaning, E_n is the energy of the neutron that is the decay partner of the nucleon N with energy E_N.

- Momentum p_N and opening angle θ_{nN} spectra

$$\Gamma_N^j = (A-2)\frac{4\mathrm{M}}{\pi}\int_{-1}^{+1} \mathrm{d}\cos\theta_{nN}\int_0^{\tilde{p}_N^j} \mathrm{d}p_N\, p_N^2\, p_n^2\mathcal{I}_N^j(p, P), \tag{18}$$

where

$$p_n = (A-1)^{-1}(p'_N - p_N\cos\theta_{nN}), \tag{19}$$

and

$$p'_N = |2\mathrm{M}(A-2)(A-1)\Delta_N^j - p_N^2[(A-1)^2 - \cos^2\theta_{nN}]|^{1/2}. \tag{20}$$

The maximum momentum of integration in (18) is

$$\tilde{p}_N^j = \sqrt{2\mathrm{M}\frac{A-1}{A}\Delta_N^j}. \tag{21}$$

This ensures that p_n, given by equation (19), is real. In order to ensure that it also be positive, as it must, one has to enforce the condition

$$p'_N > p_N\cos\theta_{nN} \tag{22}$$

throughout the integration.

Briefly, the spectra are

$$S_N^j(E_{nN}) = \frac{\mathrm{d}\Gamma_N^j}{\mathrm{d}E_{nN}} = \frac{4\mathrm{M}^3}{\pi}\sqrt{A(A-2)^3}\sqrt{(\Delta_N^j - E_{nN})(E_{nN} - \tilde{\Delta}_N^j)}\mathcal{I}_N^j(p, P), \tag{23}$$

$$S_N^j(E_N) = \frac{\mathrm{d}\Gamma_N^j}{\mathrm{d}E_N} = (A-2)\frac{8\mathrm{M}^3}{\pi}\int_{-1}^{+1}\mathrm{d}\cos\theta_{nN}\sqrt{\frac{E_N}{E'_N}}E_n\mathcal{I}_N^j(p, P), \tag{24}$$

$$S_N^j(p_N) = \frac{\mathrm{d}\Gamma_N^j}{\mathrm{d}p_N} = (A-2)\frac{4\mathrm{M}}{\pi}\int_{-1}^{+1}\mathrm{d}\cos\theta_{nN}\,p_N^2 p_n^2\mathcal{I}_N^j(p, P), \tag{25}$$

$$S_N^j(\cos\theta_{nN}) = \frac{\mathrm{d}\Gamma_N^j}{\mathrm{d}\cos\theta_{nN}} = (A-2)\frac{8\mathrm{M}^3}{\pi}\int_0^{\tilde{E}_N^j}\mathrm{d}E_N\sqrt{\frac{E_N}{E'_N}}E_n\mathcal{I}_N^j(p, P) = (A-2)\frac{4\mathrm{M}}{\pi}\int_0^{\tilde{p}_N^j}\mathrm{d}p_N\,p_N^2 p_n^2\mathcal{I}_N^j(p, P), \tag{26}$$

and

$$S_N^j(p_N, \cos\theta_{nN}) = \frac{d^2\Gamma_N^j}{\mathrm{d}p_N\,\mathrm{d}\cos\theta_{nN}} = (A-2)\frac{4\mathrm{M}}{\pi}p_N^2 p_n^2\mathcal{I}_N^j(p, P), \tag{27}$$

with p_n given by (19). The total NMWD spectra are obtained by summing on the single-particle ones, i.e. $S_N = \sum_j S_N^j$.

In order to compare our calculation results with the experimental data we will deal with the following NMWD spectra:

- proton kinetic energy spectrum

$$S_p(E_p) = \frac{\mathrm{d}\Gamma_p}{\mathrm{d}E_p}, \tag{28}$$

  where E_p is the kinetic energy of the emitted protons;
- neutron kinetic energy spectrum

$$S_{nt}(E_n) = \frac{\mathrm{d}\Gamma_{nt}}{\mathrm{d}E_n} \equiv S_p(E_n) + 2S_n(E_n), \tag{29}$$

  where $\Gamma_{nt} = \Gamma_p + 2\Gamma_n$ is the total neutron transition rate, and E_n is the kinetic energy of the emitted neutrons;

- pair kinetic energy spectrum

$$S_N(E_{nN}) = \frac{\mathrm{d}\Gamma_N}{\mathrm{d}E_{nN}}, \tag{30}$$

  where $E_{nN} \equiv E_n + E_N$ is the sum of kinetic energies of the outgoing nN pairs, and
- pair opening angle spectrum

$$S_N(\cos\theta_{nN}) = \frac{\mathrm{d}\Gamma_N}{\mathrm{d}\cos\theta_{nN}}, \tag{31}$$

  where θ_{nN} is the opening angle between n and N.

The measured spectra are obtained by counting the number of emitted nucleons $\Delta \mathrm{N}_N$ within an energy bin ΔE, or an angular bin $\Delta\cos\theta$, corrected by the detection efficiency, and normalized to the number of NMWD processes:

$$\mathrm{N}_{\mathrm{NMWD}} = \mathrm{N}_H(1 - b_m), \tag{32}$$

where N_H and b_m are, respectively, the number of produced hypernuclei and the mesonic branching ratio. (For ${}^{12}_{\Lambda}\mathrm{C}$ is $b_m = 0.232 \pm 0.012 \pm 0.005$ [15].) We note that $\Delta \mathrm{N}_N$ are of the order of thousands in the KEK experiments [13, 15, 16, 42], and of the order of hundreds in the FINUDA experiments [14, 43], with a global proton acceptance of $\epsilon_p = 0.95$ as determined in [44].

The relationship

$$\frac{\Delta \mathrm{N}_N}{\mathrm{N}_{\mathrm{NMWD}}} = \frac{\Delta\Gamma_N}{\Gamma_{\mathrm{NMWD}}} \tag{33}$$

should be fulfilled, where Γ_{NMWD} is the total NMWD decay rate, and $\Delta\Gamma_N$ is the rate of N nucleon emission within the experimentally fixed bin $\Delta E = 10$ MeV, or $\Delta\cos\theta = 0.05$ [13–15, 42, 43]. Moreover, in the case of ${}^{12}\mathrm{C}$ [13], $\Gamma_{\mathrm{NMWD}} = 0.95 \pm 0.04$, and therefore for all practical purposes one can use the approximation

$$\frac{\Delta \mathrm{N}_N}{\mathrm{N}_{\mathrm{NMWD}}} \cong \Delta\Gamma_N. \tag{34}$$

The experimental partial decay widths $\Delta\Gamma_N$ determined in this way will be confronted with the theoretical calculations obtained from the following relationships:

$$\Delta\Gamma_p(E_p) = S_p(E_p)\Delta E, \tag{35}$$

$$\Delta\Gamma_{nt}(E_n) = [S_p(E_n) + 2S_n(E_n)]\Delta E, \tag{36}$$

$$\Delta\Gamma_N(\cos\theta_{nN}) = S_N(\cos\theta_{nN})\Delta\cos\theta, \tag{37}$$

$$\Delta\Gamma_N(E_{nN}) = S_N(E_{nN})\Delta E, \tag{38}$$

where the experimental bin widths ΔE and $\Delta\cos\theta$ are the only reference to data. This is a very important difference regarding the previous work [38], where the theory has been normalized to the data, and only the kinematics entered into the play. Now we are comparing directly the theory with data, and both the kinematics and the dynamics become relevant.

In figures 1–3 the numerical calculations performed within the IPSM are presented, as well as the exchanges of complete pseudoscalar (π, K, η) and vector (ρ, ω, K^*) meson octets for the transition potential that appears in equation (8), with the weak coupling constants obtained from soft meson theorems and $SU(6)_W$ [45]. In the upper and lower panels of figure 1, respectively, the results obtained from equation (24) for inclusive proton and neutron spectra in ${}^{12}_{\Lambda}\mathrm{C}$ are shown. Besides the total spectra, the partial contributions of the $1\mathrm{s}_{1/2}$

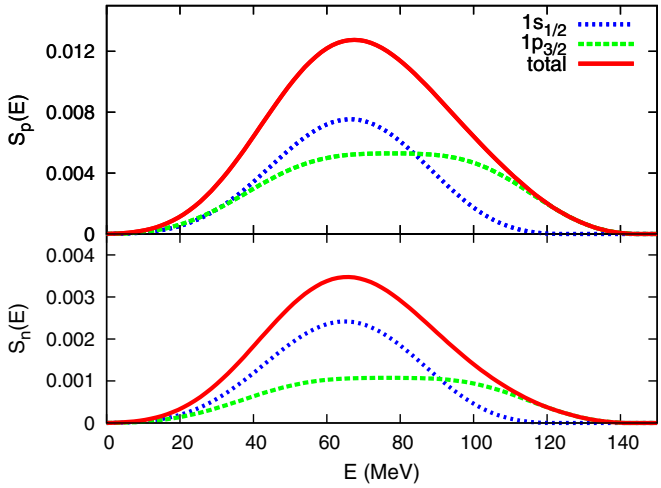

Figure 1. Inclusive kinetic energy proton and neutron spectra for $^{12}_{\Lambda}$C evaluated within the IPSM from equation (24).

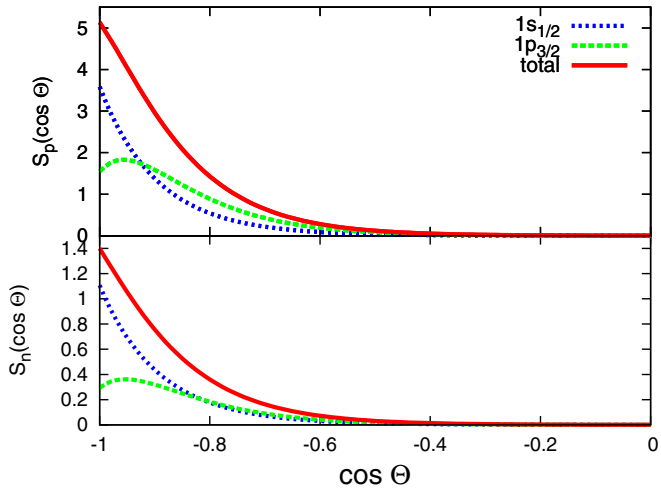

Figure 2. Opening angle correlations for proton–neutron and neutron–neutron pairs for $^{12}_{\Lambda}$C evaluated within the IPSM from equation (26).

and $1p_{3/2}$ orbitals are also shown. Similarly, in figure 2 the calculations of the opening angle correlations for proton–neutron (upper panel) and neutron–neutron pairs (lower panel) obtained by equation (26) are presented. It is worth noting that while the orbital $1s_{1/2}$ is picked at the back to back direction, the orbital $1p_{3/2}$ is not. In figure 3, the two-dimensional spectrum for protons $S(p_p, \cos\theta_{np})$ as evaluated from the IPSM with equation (27) is displayed. This spectrum, together with a similar one for neutrons, is used in this work to start the cascade process. That is, they are the main ingredients for establishing the initial condition for the evaluation of FSI by means of the many-body multicollisional Monte Carlo cascade scheme described in the next section.

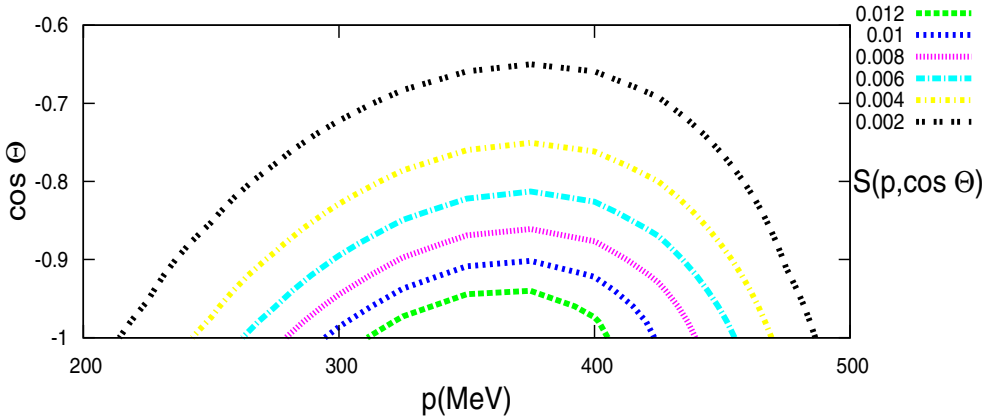

Figure 3. Two-dimensional spectrum for protons $S(p_p, \cos\theta_{np})$ as evaluated from the IPSM with equation (27).

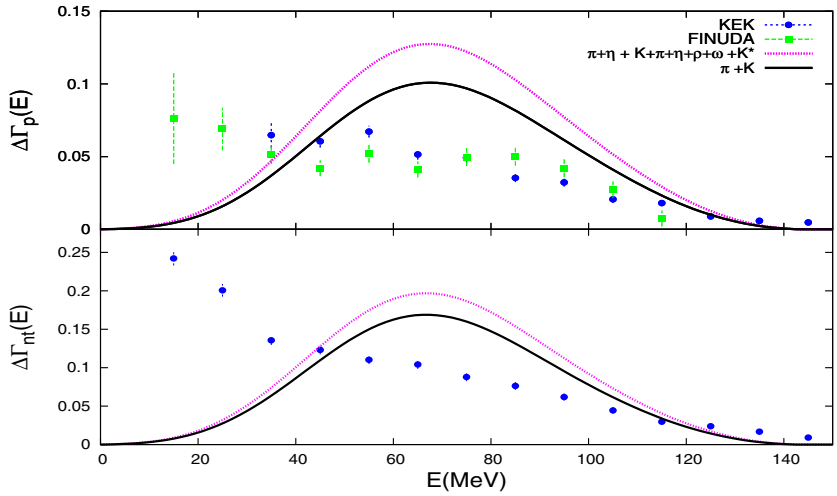

Figure 4. Comparison between the experimental and theoretical kinetic energy spectra for protons (upper panel) and neutrons (lower panel). The KEK and FINUDA experimental data are, respectively, from [16, 42] and [14, 43]. The theoretical results have been evaluated from the relations $\Delta\Gamma_p(E) = S_p(E)\Delta E$, and $\Delta\Gamma_{nt}(E) = [S_p(E) + 2S_n(E)]\Delta E$, where $\Delta E = 10$ MeV is the experimental energy bin. Two OMEP have been used: (i) the full one $\pi + K + \eta + \rho + \omega + K^*$, and (ii) the exchange of $\pi + K$ mesons only.

The IPSM calculations are confronted with KEK [13, 16, 42] and FINUDA [14, 43] experimental data in figures 4 and 5. Two OMEP have been used: (i) the full one $\pi + K + \eta + \rho + \omega + K^*$, and (ii) the exchange of $\pi + K$ mesons only. Bearing in mind that no FSI has been considered so far, the agreement with experiments is quite reasonable in the case of proton and neutron kinetic energy spectra, and specially in the case of $\pi + K$ potential, as seen in figure 4. This is not the case, however, for the angular distributions of the nN pairs shown in figure 5, where the theory overestimates the data quite significantly. It could be worth noting that both potentials yield identical spectra for the nn pairs.

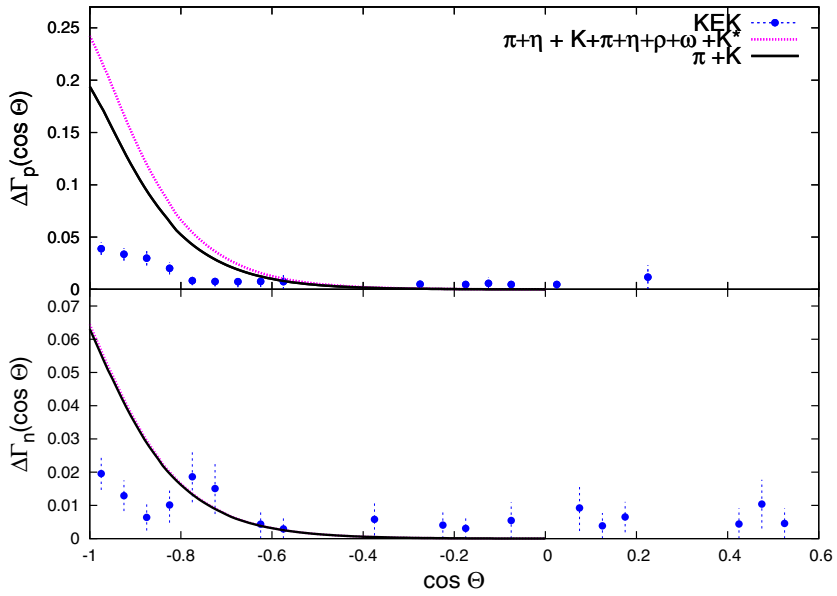

Figure 5. Comparison between experimental and calculated opening angle correlations for proton–neutron (upper panel) and neutron–neutron (lower panel) pairs. The KEK experimental data are from [15, 42]. The theoretical results have been evaluated from the relation $\Delta\Gamma_N(\cos\theta) = S_N(\cos\theta)\Delta\cos\theta$, where $\Delta\cos\theta = 0.05$ is the experimental opening angular bin. The energy cut-off $E_N > 30$ MeV has been applied in the theoretical spectra. The same OMEP were used as in figure 4.

3. FSI within the CRISP code

As a starting point for the FSI simulation, we must specify the initial configuration of the Monte Carlo sample for the decaying nucleus, and the initial positions of the A nucleons are generated to reproduce a homogeneous density distribution inside a spherical volume with radius $R = r_0 A^{1/3}$ (with $r_0 = 1.18$ fm). The energy configurations of the nucleons are determined by arrangements of A nucleons, according to the Pauli principle distributing particles in the energy levels of a potential well. The depth of the potential is properly chosen to keep the nucleons inside the nuclear volume (preventing the spurious expansion of the nuclear volume due to the Fermi motion). Afterward, a pair of nucleons is pulled out from the Fermi distribution to play the role of the two nucleons originated in the primary NMWD process. In other words, we reestablish the two-particle two-hole excitations that are present in the IPSM description. At this point, we have first to choose what is the isospin channel (neutron–proton or neutron–neutron) of this pair of nucleons. The selection is carried out taking into account the IPSM channel widths $\Gamma_N^{\rm IPSM}$. Namely, the decay channel probability of the isospin state of the nucleon pair is given by

$$R_N = \frac{\Gamma_N^{\rm IPSM}}{\Gamma_p^{\rm IPSM} + \Gamma_n^{\rm IPSM}}.$$

After deciding whether the cascade process is initiated by a neutron–neutron or a proton–neutron pair, we fix their initial momentum and angular distributions above the Fermi level by using the spectra $S_N(p)$, and $S_N(\cos\theta)$, or $S_N(p, \cos\theta)$ (see equations (25), (26), (27) and figure 3). Subsequently, the A-nucleon system evolves in time through a sequence of binary

collisions between particles, with the time step determined by the intercollisional interval of time.

We include the following elementary scattering and reaction processes.

- Elastic and inelastic nucleon–nucleon scatterings $NN \rightarrow N'N'$ with cross sections taken from [46].
- The Δ-formation process $NN \rightarrow N\Delta$ where the cross-section parametrization developed by VerWest has been used [47], while for the corresponding inverse process $N\Delta \rightarrow NN$ the extended detailed-balance relation from [48, 49] has been employed.
- The delta-resonance decay $\Delta \rightarrow \pi N$, which is governed by the characteristic exponential law.
- The pion absorption process $\pi N \rightarrow \Delta$ has been taken from a Breit–Wigner distribution function, scaled by the maximum experimental value for the inelastic cross section of the pion–nucleon reaction [50].

One should keep in mind that in the NMWD the average kinetic energy of emitted nucleons is $\simeq$ 80 MeV, and that only very few of them can reach a kinetic energy of $\simeq$ 150 MeV. Therefore, being the pion mass $m_\pi \simeq 135$ MeV, all of the mentioned reaction processes, involving pions and Δ resonance, hardly occur.

The Pauli blocking along the sequence of elementary cascade processes is taken into account by checking whether the energy levels for each resulting nucleon are available; otherwise, the elementary process in progress is blocked. During the time evolution of the cascading system, several bound nucleons are reflected on the nuclear potential surface [51, 52]. A high-energy proton can escape from the nuclear volume through refraction or tunneling through the nuclear Coulomb barrier. Low-energy protons are kept bound during subsequent nucleon–nucleon collisions, and other microscopic processes considered here. When no nucleon can escape from the spherical potential well, only low-energy collisions between particles can occur which are responsible for thermalization of the nuclear system. After reaching this equilibrium stage the effective excitation energy of the residual nucleus is determined to start the evaporation phase. In this latter phase, a chain of thermal emission of nucleons and α-particles is initiated in competition with the fission process.

The evaporation regime is governed by the relative probabilities of different particle emission channels and fission processes [53–55]. These probabilities are obtained from the particle emission width calculated according to the well-known Weisskopf evaporation model [56]

$$\Gamma_k = kT^2(E_f)\exp[S(E_f) - S(E_i)]\,, \tag{39}$$

where E_i, and E_f are, respectively, nuclear excitation energies before and after the evaporation of the particle k, which can be either a nucleon ($k = N$) or a α-particle ($k = \alpha$). $S(E_f)$ and $S(E_i)$ are the corresponding entropies, and $T(E_f)$ is the temperature of the residual nucleus (A', Z') at the end of the intranuclear cascade process. According to Weisskopf, the exponent in the above expression is given by

$$S(E_f) - S(E_i) = B_k/T(E_i), \tag{40}$$

with B_k being the separation energy of the particle k just before evaporation. In CRISP simulations, these separation energies are calculated from the liquid-drop mass formula. The temperature $T(E_f)$ is obtained from the relation

$$E(E_f) = a_k T^2(E_f), \tag{41}$$

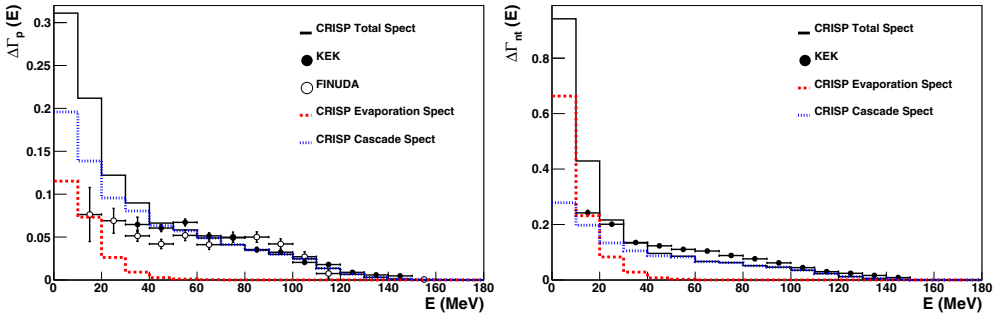

Figure 6. Calculated inclusive single-proton (left panel) and neutron (right panel) kinetic energy spectra, represented by a full histogram, are compared to the data that are the same as in figure 4. The dotted histogram is the contribution coming from the cascade regime of the process and the dashed one depicts evaporated particles from the warm post-cascade residual nucleus.

with level density parameters a_k calculated from Dostrovsky's empirical formulas [57]

$$a_N = \frac{A'}{20}\left(1 - 1.3\frac{A' - 2Z'}{A'}\right)^2, \qquad a_\alpha = \frac{A'}{20}\left(1 - \frac{3}{2Z'}\right)^2. \tag{42}$$

To evaluate the evaporation probability one assumes that it is proportional to the corresponding width, i.e.

$$P_k = \frac{\Gamma_k}{\Gamma_n + \Gamma_p + \Gamma_\alpha}. \tag{43}$$

While enough energy is available for particle evaporation, other emissions are processed. The evaporation phase ends when the excitation energy of the nucleus is smaller than all of the separation energies B_n, B_p and B_α. The CRISP code can also evaluate the fission probability in a similar procedure, but in the work presented here this contribution is not relevant. Other parameters that enter into play, such as fission barriers, and their thermal corrections, are indicated in [53–55, 58].

At the end of the whole cascade-evaporation process in the CRISP code it is possible to determine the nucleon emission originated from each phase separately, with their corresponding energy, momentum and isospin states. Consequently, we can extract from the Monte Carlo simulated events the results for the mean number of emitted protons and neutrons, as well as the angular distribution of these particles and spectra (generated separately in both phases, in cascade and evaporation). In addition, other important observable correlations between emitted particles can be obtained, such as the number of neutron–neutron or neutron–proton pairs emitted at a given opening angle. These results can be compared with similar ones calculated using only the primary NMWD model developed in the previous section. In this way, we can put in evidence the effect of the nuclear medium on the final state of the two outgoing nucleon originated from the primary process.

We report now the results obtained within the CRISP model for the inclusive single-proton and neutron kinetic energy spectra, nucleon angular distributions and energy sum spectra of neutron–proton and neutron–neutron pairs. The histograms in figure 6 show the calculated inclusive kinetic energy proton (left panel), and neutron (right panel) spectra. They exhibit a reasonable good agreement for higher energy values when compared with KEK [13, 16, 42] and FINUDA [14, 43] experimental data. The contributions coming from high-energy nucleons (originated in the cascade regime), and those from the particle evaporation process of the warm residual nucleus are shown separately. The inclusion of the latter leads to an overestimation of the experimental spectra at the low-energy region.

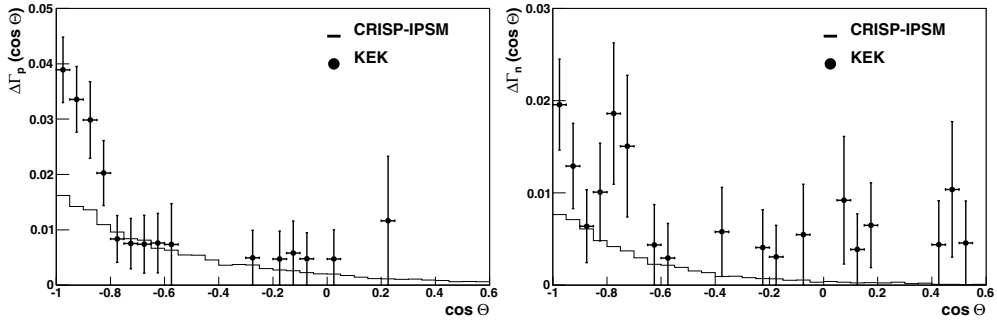

Figure 7. Angular distribution of the *np* (left panel), and the *nn* (right panel) pairs compared to experimental data in [13, 42]. These data have been reported previously in [15].

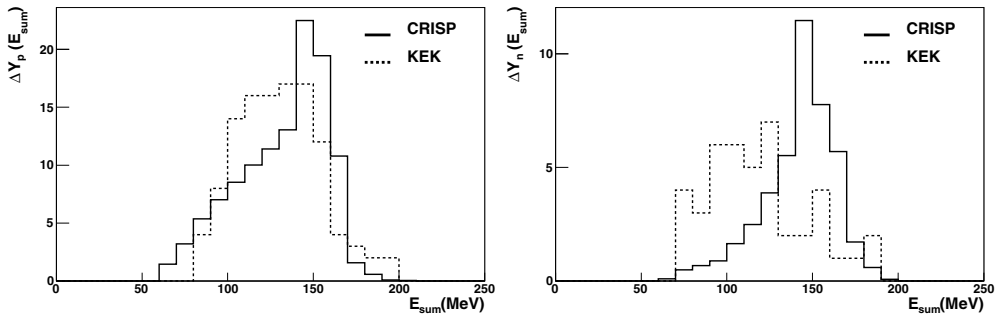

Figure 8. The kinetic energy sum distributions for *pn* (left panel) and *nn* (right panel) pairs. The dotted histogram shows data from [15], and the full histogram shows the calculated results normalized to data. We have adopted the same low-energy cutoff, and the same angle interval to define the back-to-back events as done in the experiment.

On the left and right panels of figure 7 we show the angular distributions for the *np* and *nn* channels, respectively. We get reasonable agreement with experimental results in the case of the *nn* channel, but for the *np* one our calculation does not reproduce the peak observed experimentally in the back-to-back region. We remark here that our calculation allows the break up of back-to-back correlations of *np* pairs due to the change of the proton momentum direction in the refraction process through the nuclear surface. Thus, regarding the angular distribution, we note that our FSI calculation offers a satisfactory agreement for the data in the case of correlated *nn* pairs, but still needs to be improved for correlated *np* pairs. In spite of this, the angular distribution of the primary weak decay processes is drastically modified by the inclusion of the FSI, as can be seen from the comparison of figures 5 and 7.

In figure 8 the CRISP calculation with data for the kinetic energy sum E_{nN} of the correlated nN pairs is confronted. The KEK experimental data [15] are not given for the transition rate spectra $\Delta\Gamma_N(E_{nN})$, as in the other three cases, but only for the yields $\Delta Y_N(E_{nN})$. As we do not know how to relate these two quantities with each other we are forced here to normalize the theoretical results to data in a similar way as done in [38]. Namely,

$$\Delta Y_N(E_{nN}) = \frac{\bar{Y}_N^{\exp}}{\bar{\Gamma}_N}\bar{S}_N(E_{nN})\Delta E, \tag{44}$$

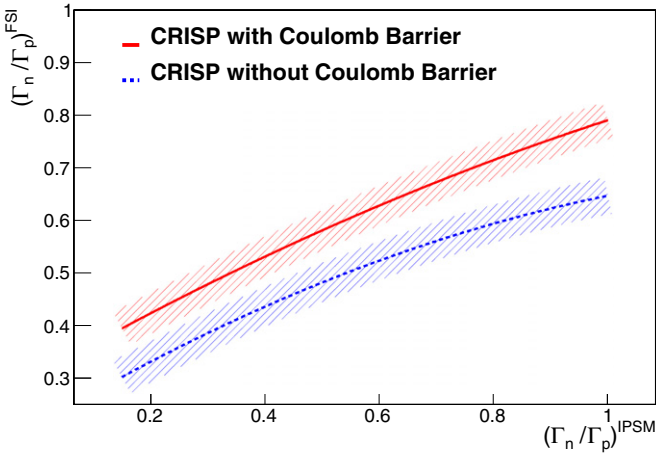

Figure 9. Behavior of $(\Gamma_n/\Gamma_p)^{\mathrm{FSI}}$ as a function of $(\Gamma_n/\Gamma_p)^{\mathrm{IPSM}}$, with and without the Coulomb barrier. The widths of the bands indicate the statistical errors involved in the Monte Carlo calculation.

where

$$\bar{Y}_N^{\mathrm{exp}} = \sum_{i=1}^{m} \Delta Y_N^{\mathrm{exp}}\left(E_{nN}^i\right), \tag{45}$$

with m being the number of kinetic energy bins $\Delta E = 10$ MeV, and

$$\bar{\Gamma}_N = \int \bar{S}_N(E_{nN})\, \mathrm{d}E_{nN} \tag{46}$$

are the calculated transition rates. The barred quantities indicate that they are constructed with events constrained to $E_N > 30$ MeV and $\cos\theta_{nN} < -0.7$. We observed that the theoretical spectrum $\Delta Y_p(E_{np})$ covers a broad energy interval going from $\simeq 60$ MeV up to the Q-value at $\simeq 165$ MeV, and that their centroid and width are quite similar to the experimental ones. For the *nn* channel, the agreement between calculated values and data is not so good. However, because of very low statistic, which in turn comes from the difficulty in detecting two neutrons in coincidence, the experimental histogram is constructed from a relatively small number of events.

Finally, we have also calculated the $(\Gamma_n/\Gamma_p)^{\mathrm{FSI}}$ ratio by considering the emitted *nn* and *np* pairs in the back-to-back opening angle region $\cos\theta_{nN} \leqslant -0.7$, obtaining the value $(\Gamma_n/\Gamma_p)^{\mathrm{FSI}} \equiv (\mathrm{Y}_n/\mathrm{Y}_p)^{\mathrm{FSI}} = 0.49 \pm 0.04$ (statistical error bar), in nice agreement with the recently reported experimental result $(\Gamma_n/\Gamma_p)^{\mathrm{exp}} = 0.53 \pm 0.13$ [15]. At this point, it is interesting to mention that our ISPM model calculation for the primary weak process yields the value $(\Gamma_n/\Gamma_p)^{\mathrm{IPSM}} = 0.26$, with the complete transition exchange potential.

The effect of the inclusion of Coulomb barrier on the ratio $(\Gamma_n/\Gamma_p)^{\mathrm{FSI}}$ is exhibited in figure 9. One sees a significant effect with the shift of the curve to higher values of $(\Gamma_n/\Gamma_p)^{\mathrm{FSI}}$ when the Coulomb barrier is included in the calculation. This is due to the non-negligible probability of having the nucleons with energies smaller than the nuclear potential depth (~ 40 MeV in our calculation) generated in the primary process. As can be seen from the upper panel in figure 4, there is a significant chance of a neutron–proton pair being originated with the proton energy around the potential depth value and hardly being detected outside the

nucleus. So the result to $(\Gamma_n/\Gamma_p)^{\mathrm{FSI}}$ increases when the barrier is incorporated to the cascade calculation.

4. Conclusions

Before discussing the effects of the FSI on the NMWD spectra we present the results for these observables in the context of the IPSM. As already mentioned in section 1, there is a quite significant difference between what is done here and in the paper of Bauer *et al* [38] since no normalization to data is performed now. In this way, both the kinematics and the dynamics are confronted, and not only the kinematics as done there.

Later on, these IPSM results are used to put in action the FSI through a time-dependent multicollisional Monte Carlo cascade scheme implemented in the CRISP (Collaboration Rio-São Paulo) code, which also includes an evaporation phase in the reaction mechanism. We have obtained fairly good agreement with experimental data of single- and double-coincidence spectra. For the inclusive nucleon spectra we have depicted the separated contributions coming from the cascade phase and from the low-energy contribution of the particle evaporation process in the post-cascade phase. In the analysis of angular distribution, we have obtained reasonable agreement for the *nn* channel, while results for the *np* channel still need to be improved in order to better account for the angular distribution. Regarding the kinetic energy sum spectra shown in figure 8, one should keep in mind that here the calculations are normalized to data and therefore the apparent agreement between the theory and data should be taken with a certain degree of caution. For a more throughout comparison we would need to have at our disposal the data on transition rates $\Delta\Gamma_N(E_{nN})$, the same as for the remaining two observables that are exhibited in figures 6 and 7.

Acknowledgments

CB and FK are fellows of CONICET, CCT La Plata (Argentina). CB thanks Agencia Nacional de Promoción Científica y Tecnológica for partial support under grant PICT-2007-00861. This work was partially supported by Argentinean agency CONICET under contract PIP 0377. SBD and AD thank CNPq for partial support. FK is grateful to Eduardo Bauer for helpful discussion and critical reading of the manuscript.

References

[1] Kubota K *et al* 1996 *Nucl. Phys.* A **602** 327
[2] Hasegawa T *et al* 1996 *Phys. Rev.* C **53** 1210
[3] Hashimoto O 1996 *Hyperfine Interact.* **103** 245
[4] Yamazaki H *et al* 1995 *Phys. Rev.* C **52** R1157
[5] Ohm H *et al* 1997 *Phys. Rev.* C **55** 3062
[6] Noumi H *et al* 1995 *Phys. Rev.* C **52** 2936
[7] Ajimura S *et al* 1994 *Nucl. Phys.* A **577** 271c
[8] Outa H 1996 *Hyperfine Interact.* **103** 227
[9] Kamagai-Fuse I, Okabe S and Akaishi Y 1996 *Phys. Rev.* C **54** 2843
[10] Savage M and Wise M B 1996 *Phys. Rev.* D **53** 349
[11] Karpeshin F F, Koutroulos C G and Grypeos M E 1995 *Nucl. Phys.* A **595** 209
[12] Riisager K 1994 *Rev. Mod. Phys.* **66** 1105
[13] Kim M J *et al* 2009 *Phys. Rev. Lett.* **103** 182502
[14] Agnello M *et al* 2010 *Phys. Lett.* B **685** 247
[15] Kim M J *et al* 2006 *Phys. Lett.* B **641** 28
[16] Okada S *et al* 2004 *Phys. Lett.* B **597** 249

[17] Ramos A, Vicente-Vacas M J and Oset E 1997 *Phys. Rev.* C **55** 735
Ramos A, Vicente-Vacas M J and Oset E 2002 *Phys. Rev.* C **66** 039903 (erratum)
[18] Garbarino G, Parreño A and Ramos A 2003 *Phys. Rev. Lett.* **91** 112501
[19] Garbarino G, Parreño A and Ramos A 2004 *Phys. Rev.* C **69** 054603
[20] Garbarino G, Parreño A and Ramos A 2005 *Nucl. Phys.* A **754** 137c
[21] Bauer E 2007 *Nucl. Phys.* A **781** 424
Bauer E 2007 *Nucl. Phys.* A **796** 11
[22] Ramos A, van Meijgaard E, Bennhold C and Jennings B K 1992 *Nucl. Phys.* A **544** 703
[23] Conti F, Meucci A, Giusti C and Pacati F D 2009 arXiv:nucl-th/09123630
[24] Barbero C, Mariano A and Duarte S B 2010 *Phys. Rev.* C **82** 067305
[25] Bauer E and Garbarino G 2009 *Nucl. Phys.* A **828** 29
Bauer E and Garbarino G 2010 arXiv:1103.2277
Bauer E and Garbarino G 2011 *Phys. Lett.* B **698** 306
[26] Gonçalves M, de Pina S, Lima D A, Milomen W, Medeiros E L and Duarte S B 1997 *Phys. Lett.* B **406** 1
[27] de Pina S, de Oliveira E C, Medeiros E L, Duarte S B and Gonçalves M 1998 *Phys. Lett.* B **434** 1
[28] Deppman A, Duarte S B, Silva G, Tavares O A P, Anefalos S, Arruda-Neto J D T and Rodrigues T 2004 *J. Phys. G: Nucl. Part. Phys.* **30** 1991
[29] Deppman A, Silva G, Anefalos S, Duarte S B, Garcia F, Hisamoto F H and Tavares O A P 2006 *Phys. Rev.* C **73** 064607
[30] Deppman A, Tavares O A P, Duarte S B, Oliveira E C, Arruda-Neto J D T, de Pina S, Likhachev V, Rodriguez O, Mesa J and Gonçalves M 2001 *Phys. Rev. Lett.* **87** 82701
[31] Tavares O A P, Duarte S B, Likhachev V and Deppman A 2004 *J. Phys. G: Nucl. Part. Phys.* **30** 37
[32] Maeda K *et al* 1994 *Nucl. Phys.* A **577** 277c
[33] Barashenkov V S, Gereghi F G, Iljinov A S, Jonsson G G and Toneev V D 1974 *Nucl. Phys.* A **231** 462
[34] Bertini H W 1963 *Phys. Rev.* **131** 1801
[35] Barbero C, Horvat D, Krmpotić F, Kuo T T S, Narančić Z and Tadić D 2002 *Phys. Rev.* C **66** 055209
[36] Krmpotić F and Tadić D 2003 *Braz. J. Phys.* **33** 187
[37] Barbero C, Galeão A P, Hussein M S and Krmpotić F 2008 *Phys. Rev.* C **78** 044312
[38] Bauer E, Galeão A P, Hussein M S, Krmpotić F and Parker J D 2009 *Phys. Lett.* B **674** 109
[39] Krmpotić F, Galeão A P and Hussein M S 2010 *AIP Conf. Proc.* **1245** 51
[40] Krmpotić F 2010 *Phys. Rev.* C **82** 055204
[41] Bauer E and Krmpotić F 2003 *Nucl. Phys.* A **717** 217
Bauer E and Krmpotić F 2004 *Nucl. Phys.* A **739** 109
[42] Bhang H 2010 private communication
[43] Garbarino G 2010 private communication
[44] Agnello M *et al* 2008 *Nucl. Phys.* A **804** 151
[45] Parreño A, Ramos A and Bennhold C 1997 *Phys. Rev.* C **56** 339
[46] Benary O, Price L R and Alexander G 1970 *N N* and *N D* interactions (above 0.5 GeV/*c*) *Report no* UCRL-20000 NN, University of California, Berkeley, CA
[47] VerWest B J and Arndt R A 1982 *Phys. Rev.* C **25** 1979
[48] Gonçalves M, Medeiros E L and Duarte S B 1997 *Phys. Rev.* C **55** 2625
[49] Wolf Gy, Cassing W and Mosel U 1992 *Nucl. Phys.* A **545** 139c
[50] Wolf Gy, Batko G, Cassing W, Mosel U, Niita K and Schäfer M 1990 *Nucl. Phys.* A **517** 615
[51] Medeiros E L, Duarte S B and Kodama T 1988 *Phys. Lett.* B **203** 205
[52] Kitazoe Y, Sano M, Yamamura Y, Furutani H and Yamamoto K 1984 *Phys. Rev.* C **29** 828
[53] Deppman A *et al* 2002 *Phys. Rev.* C **66** 067601
[54] Deppman A *et al* 2002 *Comput. Phys. Commun.* **145** 385
[55] Deppman A *et al* 2003 *Nucl. Instrum. Methods Phys. Res.* B **211** 15
[56] Weisskopf V 1937 *Phys. Rev.* **52** 295
[57] Dostrovsky I 1958 *Phys. Rev.* **111** 1659–76
[58] Anefalos S *et al* 2005 *Braz. J. Phys.* **35** 912–4